Nanoscale characterization of biomaterials

JALLOT E.

Laboratoire de Physique Corpusculaire de Clermont-Ferrand CNRS/IN2P3 UMR 6533

Université Blaise Pascal, 24 avenue des Landais 63177 Aubière Cedex France

Tel : 33 (0)4 73 40 72 65

Fax : 33 (0)4 73 26 45 98

E-mail : jallot@clermont.in2p3.fr

Keywords : Biomaterials – Interface – Physicochemical reactions – Electron microscopy – EDXS -

Table of contents

1. Introduction

'Biomaterials are defined as non-living materials able to replace a part of the human body'

Life expectancy is now over 80 years. This increase in survivability however, means that many people outlive the quality of their connective tissues and the capacity of human body to regenerate bony components that are lost or damaged is limited. Some 30 years ago, a revolution in medical care began with the successful replacement of tissues. Consequently, we have to find or to develop implants that might replace bony tissues. Two types of implants can be used : natural or synthetic [1].

The natural implants concern xenogenous, allogenous and autogenous bone grafts. Xenogenous bone grafts are implants which are coming from another species. Allogenous bone grafts are implants which are coming from the same species. However, many problems were generally associated with them such as *in vivo* resorption, virus transfer, considerable care, high costs and regular provocation of an immunological-defensive reaction, which limits their efficiency. Autogenous bone grafts are implants which are coming from the same body. These grafts are the most suitable because there is an excellent biocompatibility and no risk of transferring virus. However, removal of the bone grafts creates additional surgical trauma and its supply may not be available in sufficient quantity. To overcome all these problems, we have to find and to develop synthetic materials which might be used as bone substitutes or as prosthesis [2].

The second possibility in the revolution to replace tissues was the development, or in many cases modification, of man-made materials to interface with living, host tissues. These synthetic implants are called biomaterials. The significant advantages of synthetic implants over natural implants are availability, reproducibility and reliability. Good manufacturing

practise, international standards, government regulations and quality assurance testing minimise the risk of failure of implants. However, implants developed actually have serious disadvantages : problems of interfacial stability with host tissues, low mechanical properties, production of wear particles. These problems limits bio-integration of implants and their lifetimes. Efforts to improve properties of implants have to be done.

Actually, a lot of synthetic bone substitutes and prosthesis are available to repair bony tissues that are lost or damaged. The most widely used are polymers, metallic alloys (Ti6Al4V, Co-Cr, inox, …) and bioceramics (alumina (Al_2O_3), zirconia (ZrO_2), calcium phosphates, bioactive glasses, biovitroceramics) [3] [4]. The ultimate goal of these materials is to reach full integration of the non-living implant with living bone. With advances in ceramic technology, the application of calcium phosphate materials, bioactive glasses and biovitroceramics as bone substitutes or as coatings on prosthesis has received considerable attention, because they are highly biocompatible (well accepted in biological environment) and they have bioactive properties [5] [6] [7]. These materials are capable, through physico-chemical reactions, to establish a direct contact with bone [8]. However, many critical and complex reactions take place at the implant/bone tissues interface [9]. Structural and chemical evaluation of this interface is primordial to determine the success of an implant. Elemental composition and surface properties play a very important role in these reactions [10]. Knowledge of the elemental distribution at the biomaterials/bone tissues interface is important to understand the physico-chemical mechanisms involved during the material integration and bone bonding [11] [12].

2. Analysis of biomaterials interfaces

Structural and chemical evaluation of biomaterials/bone interfaces requires analysis at the nanometer level. Transmission electron microscopy (TEM), energy dispersive X-ray

spectroscopy (EDXS), electron energy loss spectroscopy (EELS) are methods which permits this analysis at the required resolution. TEM and associated techniques are powerful tools which can provide chemical and physical information : interlayer thickness, chemical species, local bonding, and the nature of crystalline or amorphous products [13] [14]. On the other hand, complementary techniques like PIXE (Particles induced X-ray emission), SIMS (Secondary ion mass spectrometry) and AFM (atomic force microscopy) are useful to better evaluate biomaterials/ bone tissues interface.

2.1 TEM

Development of transmission electron microscopy (TEM) permits to obtain morphological and chemical information at the nanometer scale from the sample examined. Different types of interactions can occur between incident electrons and the sample. The majority of incident electrons are transmitted, elastically diffused and inelastically diffused. Electrons are not diffused when incident electrons are transmitted without any interaction with the specimen. This phenomenon increases when the specimen thickness decreases. Electrons diffused elastically are electrons which are diffused by the electromagnetic field created by nucleus of atoms. During this interaction, they loss a very low amount of energy of the order of some eV. This diffusion is called elastic diffusion because there is no energy transferred. Electrons diffused inelastically loss energy during collisions with electrons from atoms of the sample. This energy loss is characteristic from the atoms with which this interaction occurs. Several other signals can be generated after electron beam-sample interactions : secondary electrons emission, backscattering of incident electrons, cathodoluminescence, Auger electrons emission, X-ray emission. Secondary electrons are electrons ejected from the conduction band because of their low bonding energy. Their kinetics energy is of the order of 50 eV. These electrons give a topographic information of the

surface. Backscattered electrons are electrons which pass near nucleus of atoms and are backscattered by the electromagnetic field of the nucleus. Cathodoluminescence represents photons which have a wave length between 0.4 – 0.8 μm (visible). These photons are emitted by materials like semi-conductors, organic molecules during the irradiation by the electron beam. Moreover, the interaction between the high energy electrons from the beam and atoms from the sample lead to the atoms ionisation. Electrons from the inner shells of atoms are ejected from their orbits, leaving the inner shells incompletely filled. This gap is filled by an electron from outer shells. This transition can lead to an X-ray photon emission, with an energy equal to the energy difference between the two shells or to the emission of an electron from outer shells : Auger electron.

Morphological, structural information can be obtained by contrasted images of transmitted electrons [15]. Chemical information can be obtained from the electron beam-sample interaction [15] [16]. Two of the signals generated are X-ray signal (which is used in Energy Dispersive X-ray Spectroscopy, EDXS) and electron energy loss signal issued from electrons diffused inelastically (which is used in Electron Energy Loss Spectroscopy, EELS). These two spectrometries are used to obtain elemental and eventually chemical information. EDXS is now well developed and allows the elemental analysis of all elements with Z>5. This technique permits quantitative elemental analysis, concentrations profiles and elemental cartographies with a resolution of the order of 10 nm [17]. The minimal detectable concentration is of the order of 500 ppm. EDXS allows the elemental analysis of biomaterials-tissues interface together with the study of its ultrastructure in transmission electron microscope [18] [19].

2.2 EDXS

The X-ray energy is characteristic of the element in which the electronic transition occurred and permits to determine the elements present in the sample [20]. Atoms are composed with many shells and many transition can take place [21]. The K-line correspond to an X-ray generated after the ionisation of the K-shell, the L-line correspond to an X-ray generated after the ionisation of the L shell, and so on [22]. For example, a transition from L_{III} to K is designated $K_{\alpha 1}$ and from M_V to L_{III} is designated $L_{\alpha 1}$. Transitions do not occur with the same probability. The most intense in each series are the $\alpha 1$. Considering the same line ($K_{\alpha 1}$ for example) the X-rays energy increases with the atomic number. In an atom, the K lines have a lower energy than L lines and the L lines have a lower energy than the M lines.

On the other hand, the incident electron beam can be inelastically scattered by electromagnetic field of the nucleus of atoms in the sample. The energy loss by the electron leads to an X-ray emission of corresponding energy which is called continuum or background [23]. This background do not permit to determine the elements present in the sample. However, its intensity is proportional to the mass of the analysed volume and can be used for quantitative calculations [24].

2.2.1 Instruments

A transmission electron microscope generates the electron beam and gives the ultrastructural information about the sample. The electron beam size is very important to obtain an optimal spatial resolution. Actually, scanning transmission electron microscope (STEM) permits to obtain a resolution under 1 nm. The X-rays generated in the specimen by the electron beam are collected by a semi-conductor detector, amplified and displayed with a multichannel analyser associated to a computer. Spectrum is displayed and stored.

The type of detector usually used is a lithium drifted silicon semiconductor detector (in short Si(Li) detector) cooled to liquid nitrogen temperature. The resolution of a detector is defined as the full width half-maximal height (FWHM) of the Mn K_α peak which is at an energy of 5.9 keV [25]. Actually, resolution is of the order of 140 eV. This type of detectors are protected from contamination from the microscope by a beryllium entrance window of 8 μm in thickness. However, this window absorbs low energy X-rays which limits the detection to elements heavier than Na (Z>11). Recently the developments of these detectors with an ultrathin window or window less permit the analysis of all elements down to boron.

The spectrum is composed with characteristic X-ray peaks for various elements and background (Figure 1). We can observed the presence of carbon (C K_α), oxygen (O K_α), copper (Cu L_α , Cu K_α , Cu K_β), sodium (Na K_α), silicon (Si K_α), phosphorus (P K_α) and calcium (Ca K_α , Ca K_β). Spectral lines like $\alpha 1$ and $\alpha 2$ (respectively $\beta 1$ and $\beta 2$) are so close to each other that they cannot be resolved by the spectrometer, and the convoluted line is simply denoted α (respectively β).

2.2.2 Quantitative analysis

Calculations of elemental concentrations are made in the computer. The quantitative analysis of a specimen links the characteristic X-ray intensity to the number of atoms which emit this characteristic X-ray. Two methods can be used to calculate concentrations : the Hall method [26][27][28] and the Cliff&Lorimer method [29]. In the first method, Hall proposed an alternative approach in which the mass of the matrix is measured from the intensity of the background. The concentration of an element is proportional to the peak intensity/background intensity ratio. By using standards, this method permits to quantify elemental concentrations without the detection of all elements. Concentrations are determined separately from each other. This method can be used with all types of detectors, even those with a beryllium

entrance window. However, this method has a serious disadvantage. The background of the specimen is superposed to the background of the grid support. This contribution varies with the distance between the analysed zone and the nearest bar of the grid. In order to minimize errors induced by this phenomenon, measurements must be done as far as possible from the bars of the grid. The second method does not use the background intensity. This method is based on the fact that the sum of all elemental concentrations (weight %) in the specimen is equal to unity. Then, the elemental concentration of each element can be calculated. However, this method need the correct detection of all elements present in the sample and especially light elements which are highly present in biological specimens. Detectors with a beryllium window entrance can not be used.

2.2.3 Samples preparations

For STEM and EDXS analysis at the nanometer scale the sample preparation is crucial. Several problems must be solved [30] [31].

- Ultrathin sections under 500 nm of the biomaterials-tissues interface must be prepared to perform the analysis at the resolution required. This is a very difficult step because the interface between hard materials and soft tissues must be in the sections.
- The specimen support should not contain elements of interest present in the studied sample.
- The preparation method must not change the chemical identity of the specimen. If the elements of interest in the sample are not firmly bond, they can be solubilized during preparation [32].

Actually two preparation methods can be distinguished.

a Conventional preparation method

Biological ultrathin sections are prepared by a process including different steps [33]:

- Fixation in aldehyde.
- Post-fixation in osmium (osmium tetroxide, OsO_4).
- Dehydration in increasing concentrations of alcohol.
- Embedding in resin.
- Sectioning with an ultramicrotome.
- Section staining with uranyl acetate and lead citrate.
- Carbon (C) or gold sputtering (Au).

This method allows a very good identification of the ultrastructure at the biomaterials-tissues interface [34] [35]. However, this preparation has disadvantages. Only firmly bond elements can be analysed. During fixation, the diffusible ions (Na, K, Cl, Mg, Ca) present in tissues and materials are lost from the sample [36]. During preparation, use of osmium, uranyl acetate and lead citrate adds Os, U and Pb in the sample. X-rays of these elements may interfere with X-rays of elements of interest in the sample. The gold sputtered may interfere too. Finally, chloride can be added to the sample by the resin. Table 1 summarises different types of interferences which can be generated by the sample preparation. For example, copper found in spectrum in figure 1 comes from the grid and copper is not present in the specimen.

b Cryopreparation methods

Various methods for cryopreparation are available. The first step consist of a rapid freezing of the specimen by liquid ethane cooled by liquid nitrogen (-196°C) or a metal cooled by liquid nitrogen [37] [38]. The high speed reduces considerably the formation of ice crystals. Then, cryosections are made with an ultracryomicrotome at a temperature of the order of –140°C. Then, two types of analysis are possible :

- The sections are transferred in the microscope in the frozen-hydrated state and they can be studied in this state [39] [40] [41] [42] [43].
- The sections can be freeze dried in the microscope chamber or they can be freeze dried and transferred in the microscope at the room temperature for the analysis [38].

Other techniques including freeze-drying, freeze substitution, then infiltration by resin and, finally sectioning can be used [44] [45].

These methods permit to retain all elements of interest at their *in vivo* or *in vitro* position [46] [47]. They allow to study ion distribution and ion diffusion in biomaterials during their interaction with tissues or in cells in contact with biomaterials [48]. Analysis is performed in a state near the *in vivo* or *in vitro* state.

2.3 EELS

EDXS is very useful for elemental analysis, but this technique is limited with its spatial resolution of analysis and its sensitivity. Electron Energy loss Spectroscopy (EELS) appears as a good complementary technique [49]. Its spatial resolution is of the order of the nanometer and the minimal detectable concentration in the order of 400-500 ppm. During ionisation of atoms present in the sample, electrons loss a certain amount of energy which is specific for the atoms that is ionised. Detection of energy loss by the electrons that have passed through the sample permits to determine the elemental composition and even fine structures. Sensitivity of this method for light elements is better than that of EDXS. Unfortunately, the sample must be very thin (less than 100 nm). The use of EELS is very limited for the study of biomaterials by the difficulty in preparing sufficiently thin sections.

2.4 SAED and HRTEM

High resolution transmission electron microscope (HRTEM) and electron diffraction mode, including selected-area electron diffraction (SAED) and microdiffraction permit to determine the crystalline character of a part of the studied specimens [50]. Electron beam of some nanometers in diameter are used to determine the crystalline structure. Materials are assessed as 'amorphous' when electron diffraction patterns show broad and diffuse ring patterns and when there is no visible speckle in the rings. Crystalline materials give spotty diffraction patterns or spotty ring patterns. Finally, patterns analysis and calculations allow to determine distances between atomic plans and the crystalline structure at the nanometer scale.

2.5 PIXE

Protons are charged particles which can generate characteristic X-rays in the same way as electrons do. Particles induced X-ray emission (PIXE) method used 3 MeV energy proton beam to ionise atoms. This technique is used for trace element analysis because the peak to background ratio is much better than in EDXS [51]. The limit of detection of PIXE is several ppm. A further very important advantage is that PIXE can be used as a micro-beam technique, which allows elemental mapping with a good spatial resolution. However, a proton beam can not be as finely focussed as an electron beam. Last instrumental developments permit to obtain proton beams in the order of 200-400 nm. This method is interesting to study trace elements locally at biomaterials interface.

2.6 SIMS

Secondary ion mass spectrometry (SIMS) is used to analyse the surface composition and eventually a depth profile can be obtained because several layers are sputtered away. An

ion beam is used to generate secondary ions from the surface specimen. The sensitivity of this method is of the order of 1 ppm and its resolution is near 100 nm.

2.7 AFM

During the last decade, developments of atomic force microscopy (AFM) permits to characterize the local properties of covered surfaces, namely the degree of coverage, the thickness of the layer and the shape [52]. Interactions between a tip (cantilever) and specimens surface permit to obtain images of surface structures at the nanometer scale. AFM has become a common experimental method in the investigation of biomaterials during the past 10 years [53], even if it is a delicate technique for measurements of soft materials as well as for evaluation and interpretation. This method allows to determine adsorption of proteins on materials, surface rugosities induced by protein adsorption. Concerning bioactive materials, AFM is used to study changes of surface morphology and roughness during bioactivity process. The structure of the apatite layer and the size of apatite crystals can be studied during interactions between bioactive materials and biological fluids [54] [55].

3. Physicochemical reactions at biomaterials interface

3.1 Biomaterials used to replace bony tissues

Actually, various types of biomaterials are used in orthopaedic and maxillo-facial surgery. These materials can generate different reactions at the implant/bone interface and can be separated into three categories : bio-tolerant materials, bio-inert materials and bioactive materials [56] [57] [58] [59].

3.1.1 Bio-tolerant materials

Bio-tolerant materials are materials which are incorporated in bony tissues but with interposition of a layer of fibrous tissues between the materials and bone. For example, polymethyl methacrylate and cobalt-chrome (Co-Cr) alloy. The distance between the materials and bone is in the order of 1-20 μm [60]. The presence of the fibrous layer can lead to micro-movements of the implant, to corrosion and to the release of wear debris, which limits long-term stability.

3.1.2 Bio-inert materials

Bio-inert materials are materials which are in contact with bone without leading to low tissues reactions and formation of a fibrous layer. For example : alumina (Al_2O_3), zirconia (ZrO_2), Titanium alloys [60]. However, there is no intimate or chemical contacts between bone and implants. These materials are poorly degraded by the surrounding tissues and well accepted by the biological environment. Unfortunately, sometimes wear debris are released, which limits the efficiency of the implants and its long-term stability.

3.1.3 Bioactive materials

Bioactive materials are defined by Hench [61] as materials capable to create a chemical bond with surrounding tissues without interposition of a fibrous layer. This phenomenon leads to an intimate link between bone and materials. Two kinds of bioactive materials can be defined : resorbable materials and surface reactive materials.

After implantation in bony tissues, the materials is progressively resorbed by bone cells (macrophages, osteoclasts), degraded by a chemical dissolution and finally replaced by bone [62]. Materials resorption and bone formation occurs simultaneously in order to have a

stability of the bone/materials interface [63]. The fixation of these implants is called 'biological fixation' with a porous ingrowth. These materials exhibit osteoconductive properties, defined as the characteristic of bone growth in porosities and bonding along the surface. Having the same chemical composition as natural bone, the calcium phosphate ceramics [64] (table 2) and calcium carbonates ($CaCO_3$, coral) [65] are resorbable.

The dissolution process is highly dependant of the porosity, the crystalline structure and the degree of crystallinity [66]. Calcium phosphate ceramics with macroporosities (300-400 μm) are more resorbable than calcium phosphate ceramics with microporosities (<10μm)[67] [68]. A high crystallinity degree reduces the resorbability of calcium phosphates [69]. On the other hand, it is interesting to note that some polymers are resorbable. However, mechanisms of their degradation/resorption and biological effects of their degradation products are not well known.

During the last decade, considerable attention has been directed towards use of bioactive fixation of implants. The most bioactive materials are bioactive glasses, biovitroceramics, hydroxyapatites ($Ca_{10}(PO_4)_6(OH)_2$) and composite materials (hydroxyapatite-tricalcium phosphate, …). At the interface between these materials and bone tissues a direct chemical bond is formed through a biological active apatite (Ca, P) layer [70] [71] [72]. This chemical reaction is the bioactivity property. An important advantage of bioactive fixation is that a bioactive bond to bone has a strength equal or greater than bone after 3 months. A bioactive bond to collagen fibrils of soft connective tissues is stronger than the cohesive bond of collagen fibrils. This high strength of both hard and soft tissues bonding to bioactive implants comes from the *in vivo* growth of an apatite layer of nanometer scale which bind to collagen fibrils [8].

3.2 Bioactivity process

The bioactivity process differs with the type of materials, their composition and structure. We can distinguish four types of bioactivity process.

3.2.1 Bioactivity process of bioactive glasses

In 1970, Hench [10] [73] discovers the bioactive glasses. They are amorphous materials with low mechanical properties which reduces their applications to prosthetic coatings [74] [75] and to fill bony defects [76] [77] [78] [79]. The particular composition which initiates bioactivity is based on four oxides : (45%) SiO_2, (24.5%) CaO, (24.5%) Na_2O and (6%) P_2O_5. The bioactivity properties of these materials depend on the percentage of these three oxides : SiO_2, CaO, Na_2O. An increase of SiO_2 considerably reduces the bioactivity and a high increase leads to a bio-inert material [61]. An increase of CaO or Na_2O leads to a non-glass material. In fact, a very limited range of bioactive glass compositions, containing SiO_2-CaO-Na_2O-P_2O_5, that have less than 55% SiO_2 exhibit a high bioactivity and bond to both bone and soft connective tissues [80][81]. Bioactive glasses can be obtain by melting the components at 1350°C or by sol-gel method at a lower temperature [82]. The synthesis of bioactive glasses by sol-gel process was proposed in the last decade [83] [84]. The solutions to obtain bioactive gel-glasses were prepared from stoichiometric amounts of tetraethoxysilane, triethyl phosphate and $Ca(NO_3)_2.4H_2O$. Hydrolysis and condensation at low temperature create a highly interconnected 3-D gel network composed of $(SiO_4)^{4-}$ tetrahedral via bridging oxygen bonds or by Si-O-Ca or Si-O-P non-bridging bonds [85][86][87][88].

The bioactivity process has been studied *in vitro* during interactions between bioactive glasses and biological fluids (table 3) or *in vivo* during interactions with bony tissues [12] [89] [90] [91] [92]. This process is decomposed in a complex series of physico-chemical reactions including, dissolution, diffusion, ionic exchange and precipitation (figure 2) [93] [94] [95] [96]:

- Rapid exchange of alkali ions (Na^+) with H^+ or H_3O^+ from surrounding fluids through an exchange layer of the order of 200 nm [14].

- Loss of soluble Si to the solution resulting from breaking of Si-O-Si bonds. Soluble silicon migrates toward the surface and there is formation of Si-OH and Si-$(OH)_4$ groups at the surface. The exchange process consist of a flow of H_3O^+ ions and an equivalent flow of sodium ions into the solution from the glass represented as follow :

$$SiO^-Na^+ + H_3O^+ \rightarrow SiOH + H_2O + Na^+$$

Then, there is condensation and repolymerisation of a hydrated Si rich layer on the surface depleted in alkali and Ca,P elements. This layer is a vitreous gel [54].

- Migration of Ca and P from the glass to the surface of the Si layer. Several authors described this phenomenon as a diffusion process through the Si rich layer.

- Growth of the vitreous gel by alkali exchange.

- Precipitation of an apatite (Ca-P) rich layer on top of the Si layer.

- Growth of the Ca-P rich layer. At the beginning the apatite crystals size is of the order of 200 nm and increases to some micrometers by consuming Ca^{2+}, PO_4^{3-}, CO_3^-, HPO_4^{2-} from surrounding fluids. This layer incorpores collagen fibrils from surrounding tissues.

The formation of this apatite layer represents the bioactivity properties and permits a chemical link between the materials and the newly formed bone. The apatite crystals of the Ca-P layer and the apatite crystals of bone are intermingled each others which lead to a strong bonding [97]. Concerning bioactive gel-glasses, the 1-10 nm scale solid network of the gel is completely interpenetrated by pore liquid. The pore liquid consists of a highly structured hydrated layer with hydrated connective tissues. Biological molecules can exchange with

these hydrated layers inside the pores and maintain their structure together with their biological properties [98] [99]. The nanometer sized pores of the gel glass are proposed to act as initiation sites for apatite nucleation [100].

STEM is able to show unambiguously the presence or absence of thin amorphous or crystalline films at interfaces. Figure 3 shows bioactive glass particles cultured with bone cells (osteoblasts) during two days. Interactions between bioactive glass particles and the culture medium lead to the materials dissolution, to the formation of Si layer and finally to the precipitation of an apatite layer. On the image, this layer appears as an electron dense layer. At this short time period, the apatite layer is of the order of 200 nm in thickness and its size will increases with time. In case of a crystallised apatite layer, a needle shape like structure will appear. EDXS spectrum on this layer demonstrate the presence of Ca and P elements [75]. The apatite layer acts as a template for bone cells adhesion and differenciation [91]. Figure 4 shows a bioactive glass coating/bone interface at 3 months. We clearly notice the presence of the bioactive glass coating in dissolution, the Si layer, the apatite layer and the newly formed bone. An intimate contact is observed between the glass and bone. Elemental profiles performed with EDXS permit to determine the exact composition of the different zones and their evolution with time.

One of the main problems associated with the use of bioactive glasses as prosthetic coatings is high solubility, which might reduces the long-term stability of the glass. Extensive dissolution of the glass networks occurs within days. Optimisation of bioactive glasses properties concerns the compromise between bioactivity and solubility which is related to individual components [101] [102] [103] [104]. For example, addition of Al_2O_3 can be used to control the solubility of the glass. However, this addition may inhibit the bone bonding [105].

Greenspan and Hench demonstrate that a concentration of Al_2O_3 higher than 2% inhibits bioactivity [106].

3.2.2 Bioactivity process of biovitroceramics

A vitro ceramic is obtained by a temperature treatment of a glass in which nucleation factors are added in order to induce a partial or total crystallisation of this glass. This treatment increases mechanical properties of the glass. A biovitroceramics has a structure and a particular chemical composition which are crucial for the bioactivity properties. Three types of biovitroceramics are elaborated [107] [108] :

- Biovitroceramics composed with a vitreous matrix ((16.6%) MgO, (24.2%) CaO, (59.2%) SiO_2) in which apatite crystals ($Ca_{10}(PO_4)_6(O,F_2)$ are incorporated.
- Biovitroceramics (A-W) composed with a vitreous matrix in which apatite crystals and β-wollastonite crystals ($CaSiO_3$) are incorporated.
- Biovitroceramics composed with a vitreous matrix in which apatite crystals, β-wollastonite crystals and whitelockite crystals ($3CaOP_2O_5$) are incorporated.

All these biovitroceramics contain apatite crystals which are important in the bioactivity process. Studies of the bioactivity was made *in vitro* during interactions between biovitroceramics and biological fluids, and *in vivo* during interactions between biovitroceramics and bone [108] [109]. The bioactivity is based on (figure 5) :

- Dissolution of the vitreous matrix, wollastonite crystals and whitelockite crystals (if they are incorporated).
- Ionic release of $HSiO_3^-$, Ca^{2+}, Mg^{2+} at the surface.
- Precipitation of an apatite layer by consuming Ca^{2+}, PO_4^{3-} , CO_3^- and HPO_4^{2-} from biological fluids.

The formation of this apatite layer at the surface of biovitroceramics occurs without the formation of a Si-rich layer [110] [111]. This layer of some micrometers in thickness permits a chemical bond between the materials and the newly formed bone.

3.2.3 Bioactivity process of hydroxyapatites

Synthetic hydroxyapatites are calcium phosphate ceramics elaborated under pressure and under temperature treatment of $Ca(NO_3)_2$, H_3PO_4, NH_4OH and H_2O [112]. This ceramic is used under different form : powders, bulk or as coatings. For example, figure 6 shows a STEM micrograph of nanostructures of hydroxyapatite powders. For bulk materials, various porosities are available [113]. We can distinguish microporosities (<10 μm) which permit diffusion of ions and fluids from macroporosities (100-600 μm) which permit cellular colonisation. The bioactivity process was studied *in vitro* and *in vivo* [114] [115] [116]. It occurs under an acidic attack with H^+ at the material surface (figure 7) [117]. This leads to the dissolution of hydroxyapatite crystals and a high release of Ca^{2+}, PO_4^{3-} [118] [119]. Concentration of calcium and phosphorus increase in the surrounding fluids and this supersaturation induces reprecipitation of apatite crystals at the ceramic surface [120]. These apatite crystals may incorporate Ca^{2+}, Mg^{2+}, CO_3^-, PO_4^{3-} and organic molecules present in the surrounding fluids [121] [122]. This dissolution-reprecipitation process leads to the formation of a carbonated apatite layer at the material surface and permits a chemical bond with newly formed bone [114]. This layer is in the order of 200-800 nm [123] [124] [125] [126]. Solubility of hydroxyapatites vary with different factors : porosity, grain size, crystallinity, sintering temperature [127] [128] [129] [130]. An increase of the sintering temperature leads to an increase of the hydroxyapatite crystals size and finally reduces its solubility. For example, hydroxyapatite treated at 600°C has crystals of 180 nm in size and crystals of 350

nm in size with a treatment at 1180°C [129]. On the other hand, the solubility increases with the porosity and pores size.

3.2.4 Bioactive titanium

Recently, it has been found that even pure titania hydrogel prepared by sol-gel method induces apatite formation [72] [131] [132]. When titanium is treated by immersion in alkaline solution (NaOH), a hydrated titanium oxide gel layer containing alkali ions is formed on its surface. This gel layer is dehydrated and densified to form an amorphous alkali titanate (TiO_2 + Na^+) layer by heat treatment below 600°C. When the pre-treated titanium is exposed to biological fluids, the alkali ions are released from the amorphous alkali titanate layer and hydronium ions enter into the surface layer, resulting in the formation of a titanium oxide hydrogel layer. The released Na^+ ions increase the degree of supersaturation of the soaking solution with respect to apatite by increasing pH, and titanium oxide hydrogel induces apatite nucleation on the titanium surface [133].

3.2.5 Apatite precipitation process

Determination of crystals size, nucleation and growth of apatite during interactions with surrounding fluids is important to better understand dissolution-precipitation process during bioactivity [134]. The combination of HRTEM, SAED and nano probe electron diffraction allow to determine morphology and structure of apatite crystals size [135]. The crystals size vary from a few nanometers to a micrometer [136]. The increase of the apatite crystals size occurs as a result of lower supersaturation in crystallization system because of the absence of convection in space and the strong reduction in the rate of nucleation [137].

In some cases, the apatite precipitates are amorphous. During apatite precipitation, some ions like Mg^{2+}, CO_3^- are able to enter the forming apatite nuclei and thus inhibit their

evolution to tiny apatite crystals [138]. These phenomena can promote a greater dissolution of the newly formed apatite precipitates [139] [140] [141].

4. Conclusion

Structural and chemical evaluation of bioactive biomaterials/bone tissues interface requires analysis at the nanometer scale. Transmission electron microscopy and associated techniques enable the chemical and physical characterization of bioactive materials/bone tissues interfaces, providing information on interlayer thickness, chemical species, local bonding and the nanostructural features which give rise to the interfacial properties. Thereby enabling a full understanding not only of biomaterials after processing, but also after interactions with bone tissues [142].

Bioactive materials are capable to bond directly to bone through an apatite layer. This intimate link results from simultaneous physico-chemical and biological processes. The bioactive materials in contact with bone tissues undergo dissolution with leaching and precipitation of apatite crystals occurs together with adsorption of organic compounds [143] [144]. Apatite crystals grow by epitaxial growth [145]. Simultaneously, bone cells mineralised an extracellular matrix on the materials composed with apatite crystals. Apatite crystals issued from the materials and apatite crystals issued from mineralisation are intermingled which lead to a strong bonding between implants and bone. This process of bioactivity occurs more rapidly in bioactive glasses and in biovitroceramics than in hydroxyapatite. Actually, these bioactive materials are developed and used in orthopaedic and maxillo-facial surgery.

References

1. M.B. Habal and A.H. Reddi, Bone grafts and bone substitutes, W.B. Saunders Company, Philadelphia, (1992).

2. Y. Fujishiro, L.L. Hench and H. Oonishi, J. Mater. Sci-Mater. Med. 8, 649 (1997).

3. L.L. Hench, J. Am. Ceram. Soc. 74, 1487 (1991).

4. E. Jallot, H. Benhayoune, G. Weber, G. Balossier and P. Bonhomme, J. Phys. D : Appl. Phys. 33, 321 (2000).

5. M. Jarcho, Clin. Orthop. Relat. Res. 157, 259 (1981).

6. R.Z. Legeros, Adv. Dent. Res. 2 : 164 (1988).

7. C. Ohtsuki, T. Kokubo and T. Yamamuro, J. Am. Ceram. Soc. 75, 2094 (1992).

8. L.L. Hench, Biomaterials 19, 1419 (1998).

9. T. Kitsugi, T. Nakamura, M. Oka, Y. Senaha, T. Goto and T. Shibuya, J. Biomed. Mater. Res. 30, 261 (1996).

10. L.L. Hench, R.J. Splinter, T.K. Greenlee and W.C. Allen, J. Biomed. Mater. Res. 5, 117 (1971).

11. A.M. Gatti, G. Valdre and A. Tombesi, J. Biomed. Mater. Res. 31, 475 (1996).

12. E. Jallot, H. Benhayoune, L. Kilian, J.L. Irigaray, H. Oudadesse, G. Balossier, P. Bonhomme, Surf. Interf. Anal. 29, 314 (2000).

13. M. Neo, T. Nakamura, T. Kikutani, K. Kawanabe and T. Kokubo, J. Biomed. Mater. Res. 27, 999 (1993).

14. E. Jallot, H. Benhayoune, L. Kilian, Y. Josset and G. Balossier, Langmuir 17, 4467 (2001).

15. C.C.Gray, J.N. Chapman, W.A.P. Nicholson, B.W. Robertson and R.P. Ferrier, X-ray Spectom. 12, 163 (1983).

16. J.N. Chapman, C.C.Gray, B.W. Robertson and W.A.P. Nicholson, X-ray Spectom. 12, 153 (1983).

17. J.I. Goldstein, J.L. Costley, G.W. Lorimer and S.J.B. Reed in Scanning Electron Microscopy edited O. Johari, IITRI, Chicago (1977), Vol. 1, p. 135.

18. C. Otsuki, Y. Aoki, T. Kokubo, Y. Bando, M. Neo and T. Nakamura, J. Am. Ceram. Soc. 103, 449 (1995).

19. R.Z. Legeros and G. Daculsi, Handbook of bioactive ceramics, CRC press, Boca Raton (1990), Vol. 2, p. 1.

20. C.J. Powell, Rev. Mod. Phys. 48, 33 (1976)

21. K.F.J. Heinrich, C.E. Fiori and R.L. Myklebust, J. Appl. Phys. 50, 5589 (1979).

22. A. Langenberg and J. Van Eck, J. Phys. B, 12, 1331 (1979).

23. R.H. Pratt, H.K. Tseng, C.M. Lee, and L. Kissel, A. Data Nucl. Data Tables 20, 175 (1977).

24. T.A. Hall in Physical techniques in biological research, 2nd edited G. Oster, Academic Press, New York (1971), Chap. 3.

25. P.J. Statham, X-ray Spectrom. 5,16 (1976).

26. T.A. Hall, J. Microsc. 117, 145 (1979).

27. T.A. Hall, Micron Microsc. Acta, 17, 91 (1986).

28. T.A. Hall, Scanning Micros. 3, 461 (1989).

29. G. Cliff and G.W. Lorimer, J. Microsc. 103, 203 (1975).

30. G.M. Roomans, J. Electron Microscopy Technique 9, 3 (1988).

31. K. Zierold, J. Microsc. 161, 357 (1991).

32. B.L. Gupta and T.A. Hall, Federation Proc 38, 144 (1979).

33. G. Nicaise, I. Gillot, A.K. Julliard, E. Keicher, S. Blaineau, J. Amsellem, J.C. Meyran, M.L. Hernandez-Nicause, B. Ciapa and C. Gleyzal, Scanning Microsc. 3, 199 (1989).

34. M.L. Hernandez-Nicaise, J. Amsellem, J. Ultrastruct. Res. 72, 151 (1980).

35. J.M. Sautier, D. Septier, F.J.G. Cuisinier, J.R. Nefussi, M. Oboeuf, J.C. Voegel, N. Forest and M. Goldberg, Cells and Materials 4, 357 (1994).

36. J.A. Chandler, S. Battersby in Microbeam analysis in biology edited C.P. Lechene and R.R. Warner, Academic Press, New York (1979), p. 457.

37. S. Blaineau, A.K. Julliard, J. Amsellem and G. Nicaise, Histochemistry 87, 545 (1987).

38. K. Zierold, H. Hentschel, F. Wehner and Wessing A., Scanning Microsc. Suppl. 8, 117 (1994).

39. A.T. Marshall, Scanning Electron Microsc. 2, 335 (1980).

40. A.T. Marshall in Cryotechniques in biological electron microscopy edited R.A. Steinbrecht and K. Zierold, Springer Verlag, Berlin (1987), p. 240.

41. A.T. Marshall and W. Xu, J. Microsc. 190, 305 (1998).

42. P. Echlin and S.E. Taylor, J. Microsc. 141, 329 (1986)

43. P. Echlin in Low-temperature Microscopy and Analysis, Plenum Press, New York (1992).

44. D.M.R. Harvey, J. Microsc. 127, 209 (1982).

45. D.M.R. Harvey, J.L. Hall and T.J. Flowers, J. Microsc. 107, 189 (1976).

46. A.T. Marshall, Scanning Mircrosc. Suppl. 8, 187 (1994).

47. A.T. Marshall, Scanning Electron Mircrosc., 2, 327 (1981).

48. E.M. Nkamgueu, J.J. Adnet, J. Bernard, K. Zierold, L. Kilian, E. Jallot, H. Benhayoune and P. Bonhomme, J. Biomed. Mater. Res. 52, 587 (2000).

49. R.D. Leapman and R.L Ornberg, Ultramicroscopy 24, 251 (1988).

50. E.I. Suvorova and P.A. Buffat, J. Microsc 196, 46 (1999).

51. E. Jallot, J.L. Irigaray, H. Oudadesse, V. Brun, G. Weber and P. Frayssinet, Nucl. Instrum. Meth. B 142,156 (1998).

52. M. Collaud Coen, R. Lehmann, P. Gröning, M. Bielmann, C. Galli and L. Schlapbach, J. Colloid and Interf. Sci. 233, 180 (2001).

53. A. Ikai, Surf. Sci. Rep. 26, 261 (1996).

54. E. Saiz, M. Goldman, J.M. Gomez-Vega, A.P. Tomsia, G.W. Marshall and S.J. Marshall, Biomaterials 23, 3749 (2002).

55. A. Itälä, E.C. Nordstöm, H. Ylänen, H.T. Aro and M. Hupa, J. Biomed. Mater. Res. 56, 282 (2001).

56. L.L. Hench and J.A. Paschall, J. Biomed. Mater. Res. Symp. 4, 25 (1973).

57. M. Neo, S. Kotani, T. Nakamura and T. Yamamuro J. Biomed. Mater. Res. 26, 1419 (1992).

58. M. Neo, S. Kotani, Y. Fujita, T. Nakamura and T. Yamamuro, J. Biomed. Mater. Res. 26, 255 (1992).

59. E. Jallot, J.L. Irigaray, G. Weber and P. Frayssinet, Surf. Interf. Anal. 27, 648 (1999).

60. J.F. Osborn and H. Newesely, in dynamic aspect of the implant/bone interface edited G. Heimke, Cark Hansen Verlag, Germany (1980), p. 111.

61. L.L. Hench in Handbook of bioactive ceramics edited T. Yamamuro, L.L. Hench and J. Wilson, CRC Press, Boca raton (1990), Vol. 1, p. 7.

62. E. Jallot, J.L. Irigaray, H. Oudadesse, V. Brun, G. Weber and P. Frayssinet, Eur. Phys. J. AP 6, 205 (1999).

63. G. Daculsi, R.Z. Legeros, E. Nery and K. Lynch, J. Biomed. Mater. Res. 23, 883 (1988).

64. R.Z. Legeros, Clinical Materials 14, 65 (1993).

65. C.J. Damien, J.L. Ricci, P. Christel, H. Alexander and J.L. Patat, Calcified Tissue Int. 55, 151 (1994).

66. G. Daculsi, R.Z. Legeros and D. Mitre, Calcified Tissue Int. 46, 20 (1990).

67. H. Benhayoune, E. Jallot, P. Laquerrière, G. Balossier, P. Bonhomme and P. Frayssinet, Biomaterials 21, 235 (2000).

68. C.P.A.T. Klein, A.A. Driessen, K. De Groot and A. Van Den Hoof, J. Biomed. Mater. Res. 17, 769 (1983).

69. C.P.A.T. Klein, A.A. Driessen and K. De Groot, Biomaterials 5, 157 (1984).

70. K.J.J. Pajamaki, T.S. Lindholm and O.H. Andersson, J. Mater. Sci-Mater. Med. 6, 14 (1995).

71. U. Gross and V. Strunz, J. Biomed. Mater. Res. Symp. 7, 503 (1985).

72. L. Jonasova, F.A. Müller, A. Helebrant, J. Strnad and P. Greil, Biomaterials 23, 3095 (2002).

73. L.L. Hench, Med. Inst. 57, 136 (1973).

74. R.J. Furlong and J.F. Osborn, J. Bone Joint Surg. 77, 534 (1995).

75. A. Merolli, A. Cacchioli, L. Giannotta and P. Tranquilli Leali, J. Mater. Sci-Mater. In Med. 12, 727 (2001).

76. E. Shepers, M. De Clerq, P. Ducheyne and R. Kempeneers, J. Oral Rehabil. 18, 439 (1991).

77. L.L. Hench and J.K. West, Life Chem. Rep. 13, 187 (1996).

78. Ö.H. Andersson, K.H. Karlsonn and K. Kangasniemi, J. Non-Cryst. Solids 119, 290 (1990).

79. Ö.H. Andersson, G. Liu, K. Kangasniemi, J. Juhanoja, J. Mater. Sci-Mater. in Med. 3, 145 (1992).

80. W. Cao and L.L. Hench, Ceramics Int. 22, 493 (1996).

81. O. Peitl, E.D. Zanotto and L.L. Hench, J. Non-cryst. Solids 292, 115 (2001).

82. W. Gong, A. Abdelouas and W. Lutze, J. Biomed. Mater. Res. 54, 320 (2001).

83. R. Viitala, M. Jokinen, T. Peltola, K. Gunnelius and J.B. Rosenholm, Biomaterials 23, 3073 (2002).

84. C. Kinowski, M. Bouazaoui, R. Bechara, L.L. Hench, J.M. Nedelec and S. Turell, J. Non-cryst. Solids, 291, 143 (2002).

85. L.L. Hench and R. Orefice in Kirk-Othmer encyclopedia of chemical technology, Wiley, New York, (1997) 4th ed., Vol. 22., p. 497.

86. R. Li, A.E. Clark and L.L. Hench in Chemical processing of advanced materials edited L.L. Hench and J.K. West, Wiley, New York, (1992), p. 627.

87. M.M. Pereira, A.E. Clark and L.L. Hench, J. Mater. Synth. Proc. 2, 189 (1994).

88. M.M. Pereira, A.E. Clark and L.L. Hench, J. Biomed. Mater. Res. 18, 693 (1994).

89. L.L. Hench and J. Wilson, Science 226, 630 (1984).

90. C.Y. Kim, A.E. Clark and L.L. Hench, J. Non-Cryst. Solids 113, 195 (1988).

91. C. Loty, J.M. Sautier, M.T. Tan, M. Oboeuf, E. Jallot, H. Boulekbache, D. Greenspan and N. Forest, J. Bone Miner. Res. 16, 231 (2001).

92. A. El Ghannam, Ducheyne P and I.M. Shapiro, J. Biomed. Mater. Res. 29, 359 (1995).

93. I.D. Xynos, A.J. Edgar, L.D.K. Buttery, L.L. Hench and J.M. Polak, Biochem. Bioph. Res. Co. 276, 461 (2000).

94. W.C.A. Vrouwenvelder, G.C. Groot and K. De Groot, Biomaterials 13, 382 (1992)

95. A. El Ghannam, Ducheyne P and I.M. Shapiro, Biomaterials 18, 295 (1997).

96. E. Jallot, H. Benhayoune, L. Kilian, J.L. Irigaray, Y. Barbotteau, G. Balossier and P. Bonhomme, J. Colloid Interf. Sci. 233, 83 (2001).

97. O. Pietrement and E. Jallot, Nanotechnology 13, 18 (2002).

98. D. Avnir, L.C. Klein, D. Levy, U. Schubert and A.B. Wojcik in The chemistry of organosilicon compounds edited Y. Apeloig and Z. Rappoport, Wiley, Chichester, (1997), part. 2.

99. J. Livage, C. Roux, J.M. Da Costa, I. Desportes and J.E. Quinson, J. Sol-Gel Sci. Technol. 7, 45 (1996).

100. J.R. Jones and L.L. Hench, Materials Science and technology 17, 891 (2001).

101. C. Ohtsuki, T. Kokubo and T. Yamamuro, J. Non-cryst. Solids 143, 84 (1992).

102. U. Gross and V. Strunz, J. Biomed. Mater. Res. Symp. 7, 503 (1985).

103. M. Vallet-Regi, I. Izquierdo-Barba and A.J. Salinas, J. Biomed. Mater. Res. 46, 560 (1999).

104. M. Ogino, F. Ohuchi and L.L. Hench, J. Biomed. Mater. Res. 14, 55 (1980).

105. K. Kangasniemi and A. Yli-Urpo in Handbook of Bioactive Ceramics edited J. Wilson, CRC Press, Boston (1990), Vol. 1, p. 97.

106. D.C. Greenspan and L.L. Hench, J. Biomed. Mater. Res. 10, 503 (1976).

107. T. Kokubo, H. Kushitani, C. Ohtsuki, S. Sakka and T. Yamamuro, J. Mater. Sci-Mater. Med. 3, 79 (1992).

108. T. Kokubo, S. Ito, Z.T. Huang, T. Hayashi, S. Sakka, T. Kitsugi and T. Yamamuro, J. Biomed. Mater. Res. 24, 331 (1990).

109. P. Li, C. Ohtsuki, T. Kokubo, K. Nakanishi, N. Soga, T. Nakamura and T. Yamamuro, J. Am. Ceram. Soc. 75, 2094 (1992).

110. T. Kokubo, Biomaterials 12, 155 (1991).

111. T. Kokubo, J. Ceram. Soc. Jpn. 99, 965 (1991).

112. R. Aoba and E.C. Moreno, J. Dent. Res. 63, 874 (1984).

113. P.S. Eggli, W. Muller and R.K. Schenk, Clin. Orthopd. Relat. R. 232, 127 (1988).

114. R.Z. Legeros and G. Daculsi, in Handbook of bioactive ceramics edited T. Yamamuro, L.L. Hench and J. Wilson, CRC Press, Boca raton (1990), Vol. 2, p. 17.

115. I. Orly, M. Gregoire, M. Menanteau and M. Dard, Adv. Biomater. 8, 211 (1988).

116. E. Jallot, Med. Eng. Phys. 20, 697 (1998).

117. G. Daculsi, G. Kerebel and L.M. Kerebel, Caries Res. 13, 277 (1979).

118. G. Daculsi, R.Z. Legeros and D. Mitre, Calcified Tissue Int. 45, 95 (1989).

119. R.Z. Legeros, I. Orly, M. Gregoire and J. Kaimiroff, J. Dent. Res. 67, 177 (1988).

120. I. Orly, M. Gregoire, M. Menanteau, M. Heughebaert and B. Kerebel, Calcified Tissue Int. 45, 20 (1989).

121. R.Z. Legeros, M.H. Taheri, G.M. Quirolgico and J.P. Legeros, Scanning Electron Microsc. 407 (1983).

122. R.Z. Legeros, R. Kijkowska, T. Abergas and J.P. Legeros, J. Dent. Res. 65, 293 (1986).

123. H.N. Denissen, K. De Groot, P.C. Makkes, A. Van Den Hoof and P.J. Klopper, J. Biomed. Mater. Res. 14, 730 (1980).

124. J.M. Sautier, J.R. Nefussi and N. Forest, Cells and Materials 1, 209 (1991).

125. J.M. Sautier, J.R. Nefussi and N. Forest, Biomaterials 12, 400 (1992).

126. G.C.L. De Lange, C. De Putter and F.L.J.A. De Wijs, J. Biomed. Mater. Res. 24, 829 (1990).

127. K. De Groot, Ann. New York Acad. Sci. 523, 227 (1988).

128. R.Z. Legeros and X. F. Chang, J. Dent. Res. 68, 215 (1989).

129. P. Laquerrière, L. Kilian, A. Bouchot, E. Jallot, A. Grandjean, M. Guenounou, G. Balossier, P. Frayssinet and P. Bonhomme. J. Biomed. Mater. Res. 58, 238 (2001).

130. O. Malard, J.M. Bouler, J. Guicheux, D. Heymann, P. Pilet, C. Coquard, G. Daculsi, J. Biomed. Mater. Res. 46, 103 (1999).

131. P. Li, C. Ohtsuki, T. Kokubo, K. Nakanishi, N. Soga and K. De Groot, J. Biomed. Mater. Res. 28, 7 (1994).

132. P. Li, I. Kangasniemi, K. De Groot and T. Kokubo, J. Am. Ceram. Soc. 5, 1307 (1994).

133. T. Kokubo, F. Miyaji and H.M. Kim, J. Am. Ceram. Soc. 4, 1127 (1996).

134. G. Daculsi, R.Z. Legeros, J.P. Legeros, D. Mitre, J. Biomed. Mater. Res. 2, 147 (1991).

135. E.I. Suvorova and P.A. Buffat, J. Microsc. 196, 46 (1999).

136. H.E. Lundager Madsen, F. Christensson, L.E. Polyak, E.I. Suvorova, M.O. Kliya and A.A Chernov, J. Cryst. Growth 152, 191 (1995).

137. E.I. Suvorova, F. Christensson, H.E. Lundager Madsen, A.A. Chernov, J. Cryst. Growth 186, 262 (1998).

138. G. Daculsi, R.Z. Legeros, M. Heughebaert and I. Barbieux, Calcified Tissue Int. 46, 20 (1990).

139. E. Jallot, H. Benhayoune, L. Kilian, J.L. Irigaray, G. Balossier and P. Bonhomme, J. Phys. D : Appl. Phys. 33, 2775 (2000).

140. R.Z. Legeros in Tooth enamel IV edited R.W. Fearnhead and S. Suga, Elsevier, Amsterdam (1984), p. 32.

141. R.Z. Legeros and R. Kijkowska, J. Dent. Res. 68, 1003 (1989).

142. E. Verne, C. Vitale Brovarone, C. Moisescu, E. Ghisolfi and E. Marmo, Acta Mater. 48, 4667 (2000).

143. L.L. Hench in the Bone-Biomaterials interface edited J.E. Davies, University of Toronto Press, Toronto (1991), p. 33.

144. B. Kasemo and J. Lausmaa in the Bone-Biomaterials interface edited J.E. Davies, University of Toronto Press, Toronto (1991), p. 19.

145. R.Z. Legeros, I. Orly, M. Gregoire and G. Daculsi in the Bone-Biomaterials interface edited J.E. Davies, University of Toronto Press, Toronto (1991), p. 76.

Tables captions

Table 1 : Common extraneous peaks causing artefacts during analysis.

Table 2 : Some calcium phosphates available actually.

Table 3 : Ion concentrations ($mmol.dm^{-3}$) of biological solutions used to study physico-chemical reactions of bioactive materials.

Extraneous peak	Source	Interferes with these elements
Al K_α	Specimen holder	Br L_α
Si K_α	Contamination from microscope	Sr L_α
Cu K_α	Grid	Zn K_α , Os L_α
Cu L_α	Grid	Na
Pd L_α	Coating	Cl K_α
Pd L_β	Coating	K K_α
Os L_α	Postfixation	Zn K_α
Os M_α	Postfixation	P K_α
Au M_α	Coating	P K_α , S K_α
Pb M_α	Section staining	S K_α , Cl K_α
U M_α	Section staining	K K_α

Table 1

Calcium phosphates (synthetic)	Chemical formulae	Ca/P
Brushite, dicalcium phosphate dihydrate	$CaHPO_4.H_2O$	1
Monetite, dicalcium phosphate anhydrous	$CaHPO_4$	1
Octacalcium phosphate, OCP	$Ca_8H_2(PO_4)_6.5H_2O$	1.33
Tricalcium phosphate, β-TCP	$Ca_3(PO_4)_2$	1.5
Calcium hydroxyapatite, HA	$Ca_{10}(PO_4)_6(OH)_2$	1.67
Calcium fluorapatite, FA	$Ca_{10}(PO_4)_6F_2$	1.67
Tetracalcium phosphate	$Ca_4P_2O_9$	2

Table 2

	Na^+	K^+	Mg^{2+}	Ca^{2+}	Cl^-	HCO_3^-	HPO_4^{2-}	SO_4^{2-}
Simulated body fluid, SBF	142	5	1.5	2.5	147.8	4.2	1	0.5
Human plasma	142	5	1.5	2.5	103	27	1	0.5

Table 3

Figures captions

Figure 1 : Spectrum showing characteristic peaks for various elements and the continuum (background).

Figure 2 : Schematic view of the bioactive glass/bone interface during the bioactivity process.

Figure 3 : STEM micrograph of bioactive glass particles immersed in a biological solution with bone cells (osteoblasts) during two days. The particles are in dissolution and an electron dense layer appears (apatite layer). These particles are engulfed in an organic matrix.

Figure 4 : STEM micrograph of a bioactive glass coating/bone interface after 3 months of implantation. The bioactive glass coating is in dissolution and firmly fixed to newly formed bone through an apatite layer on top of a pure Si layer.

Figure 5 : Schematic view of the biovitroceramic/bone interface during the bioactivity process.

Figure 6 : TEM micrograph showing nanostructures of hydroxyapatite particles.

Figure 7 : Schematic view of the hydroxyapatite/bone interface during the bioactivity process.

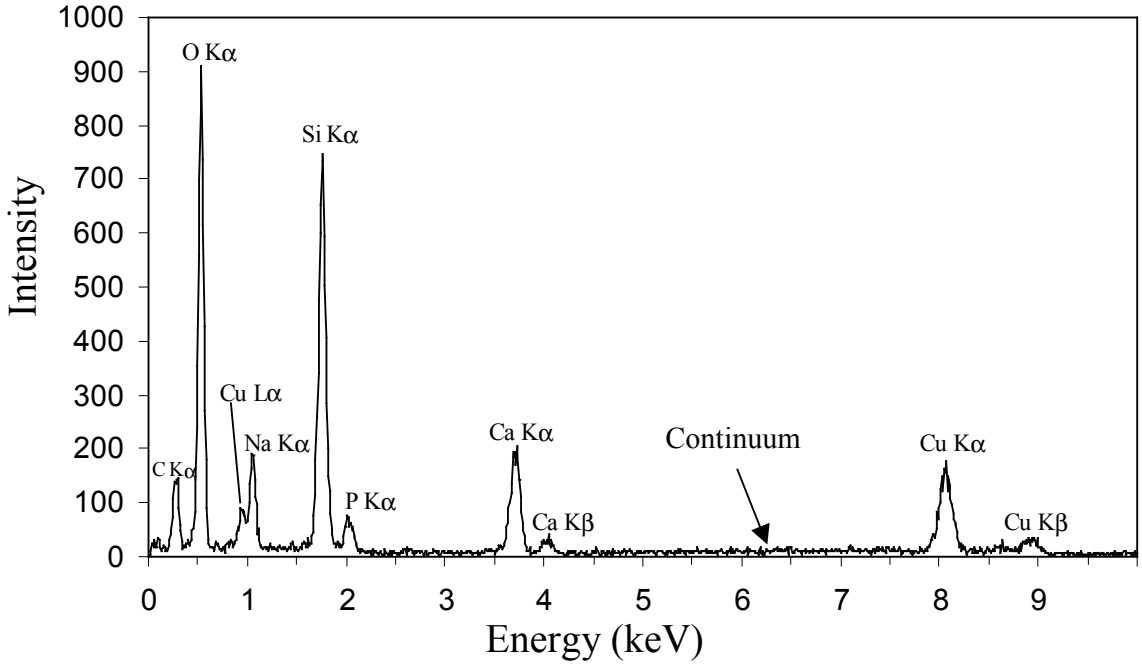
Intensity
Energy (keV)
O Kα
Si Kα
Cu Lα
Na Kα
C Kα
P Kα
Ca Kα
Ca Kβ
Continuum
Cu Kα
Cu Kβ
0
100
200
300
400
500
600
700
800
900
1000
0
1
2
3
4
5
6
7
8
9

Figure 1

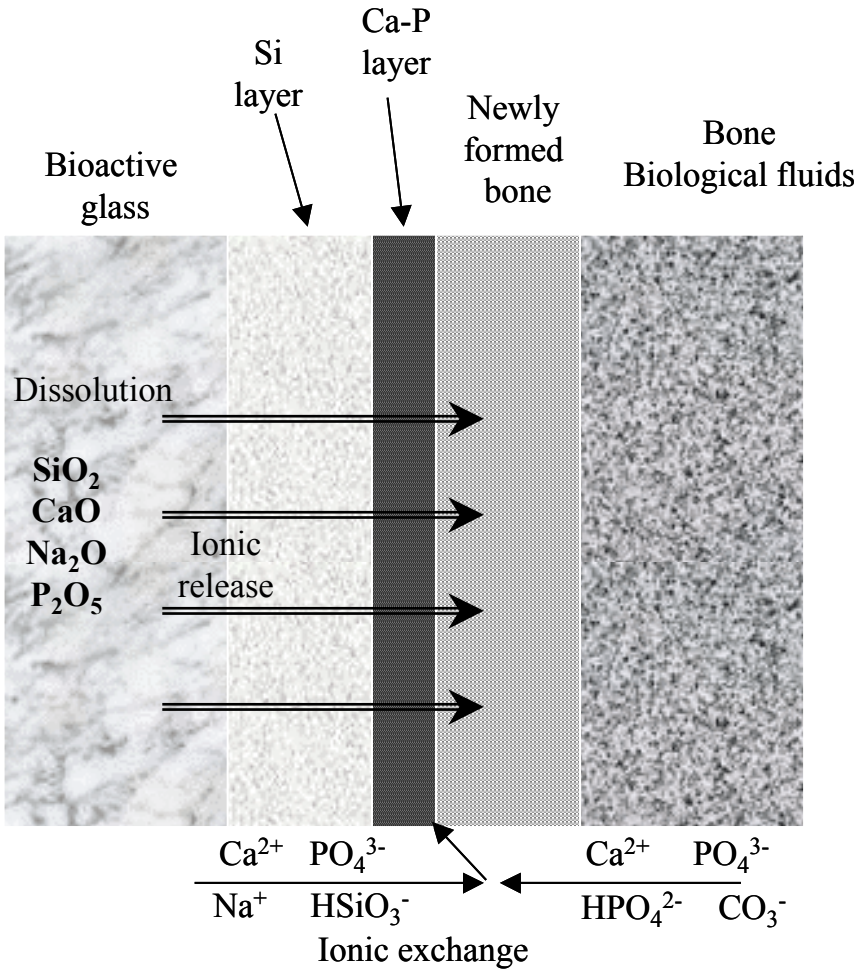
Ca-P
layer
Si
layer
Newly
formed
bone
Bone
Biological fluids
Bioactive
glass
Dissolution
SiO_2
CaO
Na_2O
P_2O_5
Ionic
release
Ca^{2+} PO_4^{3-}
Na^+ $HSiO_3^-$
Ca^{2+} PO_4^{3-}
HPO_4^{2-} CO_3^-
Ionic exchange

Figure 2

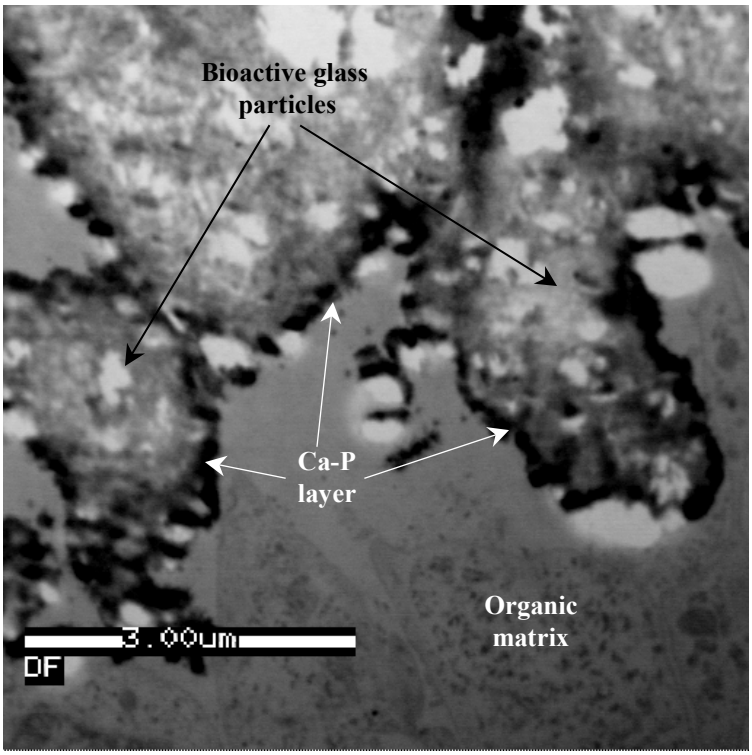

Figure 3

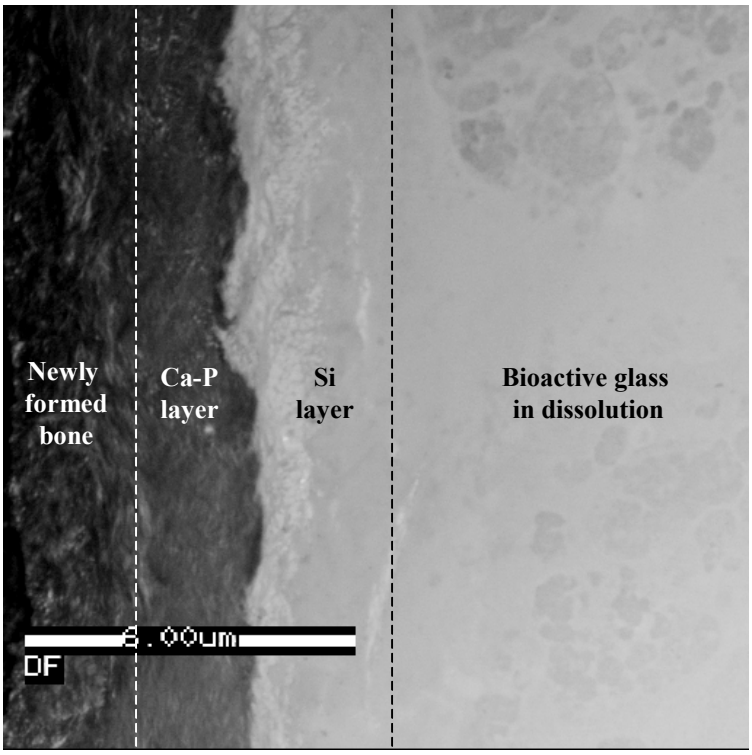

Figure 4

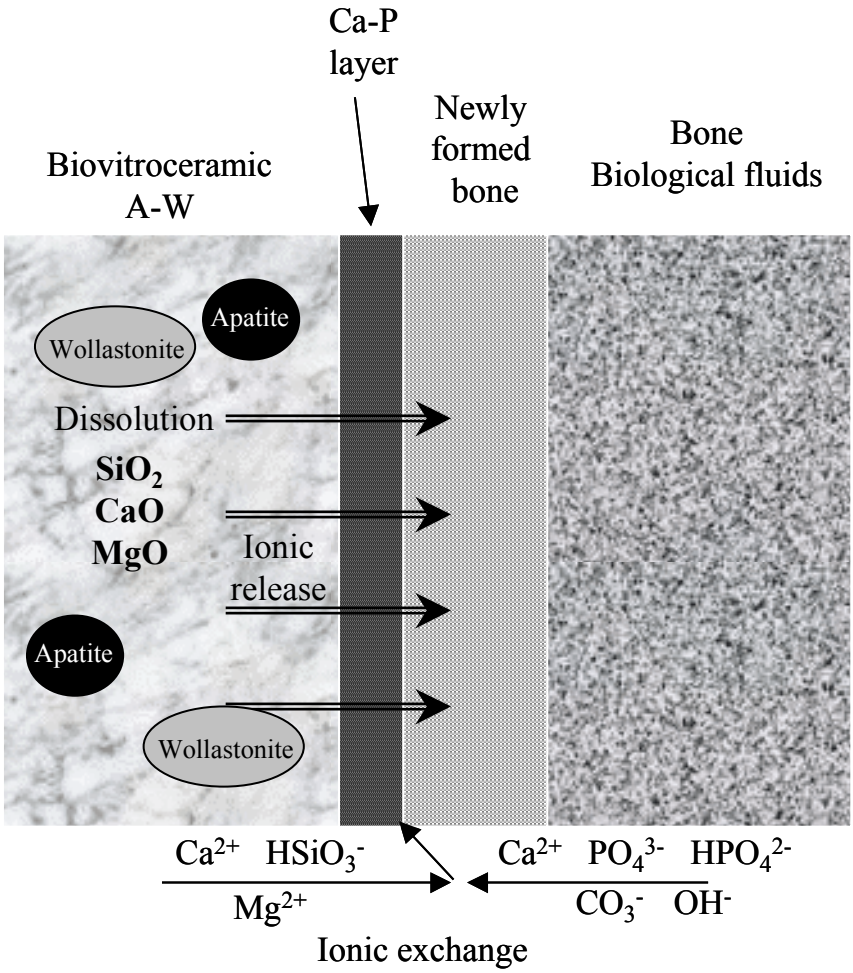
Ca-P
layer
Newly
formed
bone
Bone
Biological fluids
Biovitroceramic
A-W
Apatite
Wollastonite
Dissolution
SiO2
CaO
MgO
Ionic
release
Apatite
Wollastonite
Ca2+ HSiO3-
Mg2+
Ca2+ PO43- HPO42-
CO3- OH-
Ionic exchange

Figure 5

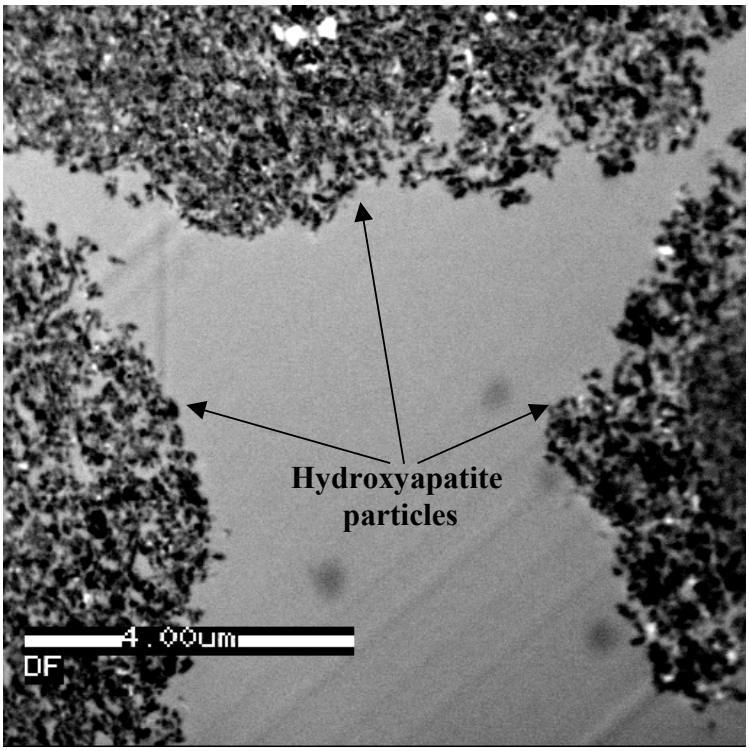

Figure 6

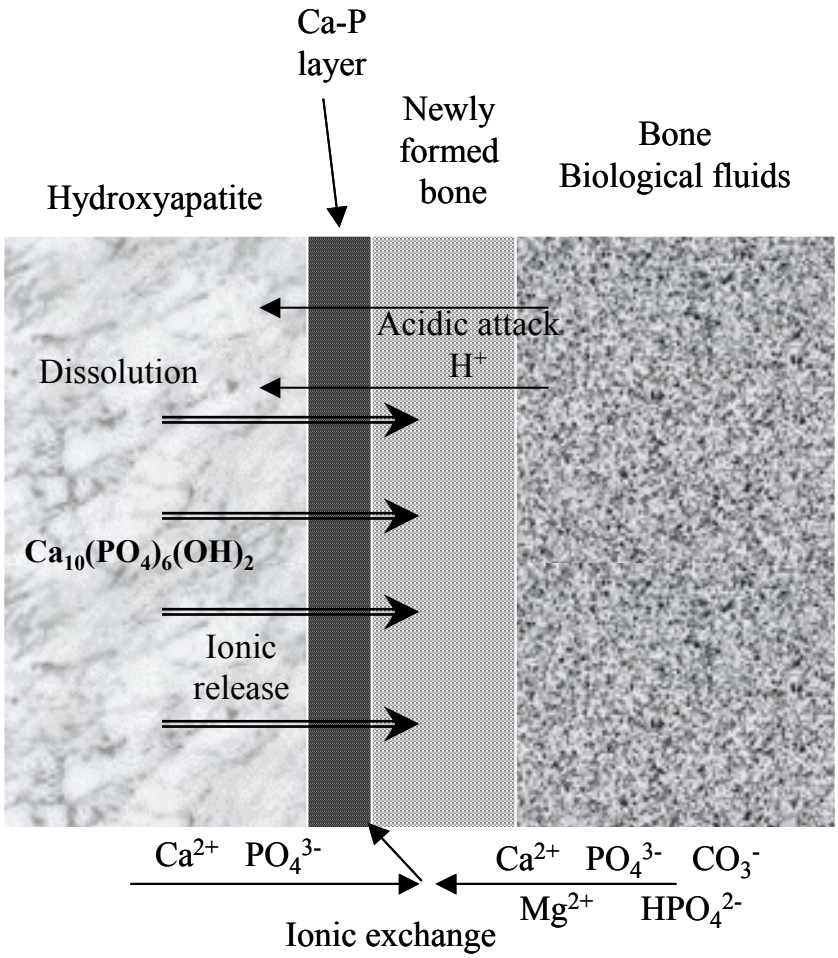
Ca-P
layer
Newly
formed
bone
Bone
Biological fluids
Hydroxyapatite
Acidic attack
H+
Dissolution
Ca10(PO4)6(OH)2
Ionic
release
Ca2+ PO43-
Ca2+ PO43- CO3-
Mg2+ HPO42-
Ionic exchange

Figure 7